High visible light photocatalytic activity of nitrogen-doped ZnO thin films deposited by HiPIMS

Vasile Tiron, Ioana-Laura Velicu, Dana Stanescu, Helene Magnan, Lucel Sirghi

Surface & Coatings Technology xxx (2016) xxx–xxx

Contents lists available at ScienceDirect

Surface & Coatings Technology

journal homepage: www.elsevier.com/locate/surfcoat

High visible light photocatalytic activity of nitrogen-doped ZnO thin films deposited by HiPIMS

Vasile Tiron [a], Ioana-Laura Velicu [a], Dana Stanescu [b], Helene Magnan [b], Lucel Sirghi [a,*]

[a] Iasi Plasma Advanced Research Center (IPARC), Faculty of Physics, "Alexandru Ioan Cuza" University of Iasi, Iasi 700506, Romania
[b] SPEC, CEA, CNRS, Université Paris-Saclay, CEA-Saclay, 91191 Gif-sur-Yvette Cedex, France

ARTICLE INFO

Article history:
Received 31 May 2016
Revised 7 November 2016
Accepted in revised form 23 November 2016
Available online xxxx

Keywords:
HiPIMS deposition
N-doped ZnO
Visible-light photocatalyst
Water splitting

ABSTRACT

Reactive High Power Impulse Magnetron Sputtering (HiPIMS) of a pure Zn target in $Ar/N_2/O_2$ gas mixture was used to synthesize ZnO_xN_y thin films with nitrogen content and optical band-gap energy values ranging over 0–6.2 at.% and 3.34–1.67 eV, respectively. The fine control of the nitrogen content in the deposited ZnO_xN_y thin films composition was possible through the stabilization of the reactive HiPIMS discharge in the transition region, between the metallic and compound target sputtering modes. Various analytical techniques such as AFM, XPS, XRD, UV–Vis and Raman spectroscopy have been employed to characterize the properties of the deposited thin films. The photocatalytic activity, light excitation efficiency and life time of photo-generated charge carriers in the ZnO_xN_y films were investigated by photo-electrochemical and photo-current measurements during visible light on/off irradiation cycles. The as-deposited films showed poor visible-light photocatalytic activity and photo-current response. Post-deposition annealing of the films in nitrogen atmosphere resulted in a slight enhancement of crystalline order. However, the thermal treatment improved considerably the film photocatalytic activity and stability for water splitting under visible light irradiation. The optimum photo-current response and photocatalytic activity have been obtained for the annealed ZnO_xN_y films with a nitrogen content of 3.4 at.% (photon-to-current efficiency up to 33% at $\lambda = 370$ nm and 0.5 V biasing potential vs. Ag/AgCl). Increasing the nitrogen content above this value, in spite of lowering the energy band-gap, worsened the visible light photocatalytic activity of the films due to deterioration of the crystalline order.

1. Introduction

Metal oxide semiconductors hold great promise for application in conversion of solar to chemical energy by photo-catalysis. However, critical factors such as inability to utilize visible light efficiently, fast recombination of photo-generated electron-hole pairs and quick backward reaction have restricted other possible practical and viable applications [1]. Therefore, improving photocatalytic performance of metal oxide semiconductors by narrowing the optical band-gap to make possible absorption in the visible region and to inhibit the recombination of photo-generated electron-hole pairs has become a hot topic among researchers in the recent years. A variety of strategies was proposed to overcome these drawbacks, including: (*i*) doping of wide-band-gap oxides with different elements to shift their photocatalytic response to the visible light region [2]; (*ii*) use of nanopatterned thin films to confine the photo-excited charge carriers at surface and to increase the specific active surface [3]; and (*iii*) use of co-catalyst particulate metals for electron trapping [4].

Nitrogen doped ZnO proved to be a good photocatalytic material due to its enhanced light absorption and transport of photo-generated charge carriers [5]. Reducing the optical band-gap and inhibiting the recombination of photo-generated electron-hole pairs by nitrogen doping are key strategies to successfully synthesize ZnO based visible-light photocatalyst. In a previous work [6], we have investigated the ability of reactive short-pulse High Power Impulse Magnetron Sputtering (HiPIMS) technique to tailor the chemical composition of ZnO_xN_y thin films. It has been proved that the nitrogen content of the deposited ZnO_xN_y thin films can be finely controlled by changing the HiPIMS pulsing frequency in the transition region from the compound to the metallic target sputtering mode. Increasing the HiPIMS pulsing frequency resulted in transition towards the metallic target sputtering mode with a significant increase in the amount of sputtered metal in the gas phase. In these conditions, using a low fraction of oxygen in the working gas mixture favored incorporating the nitrogen in the ZnO_xN_y films deposited at room temperature. It worth mentioning that deposition on heated substrates yielded ZnO_xN_y films with very low or no content of nitrogen. Due to the very high electron density in HiPIMS, both sputtered metal flux and reactive gas flux are highly ionized, leading to an increased reactivity at the film's surface and a better and easier

* Corresponding author.
E-mail address: lsirghi@uaic.ro (L. Sirghi).

http://dx.doi.org/10.1016/j.surfcoat.2016.11.087
0257-8972/

control of the elemental and phase composition of the compound films [7,8].

In the present work, reactive short-pulse HiPIMS is used to synthesize nitrogen-doped zinc oxide (ZnO_xN_y) thin films with narrow optical band-gap and good photocatalytic activity in the visible light. The optical and structural properties of the deposited ZnO_xN_y thin films were investigated through Ultraviolet-Visible (UV–Vis), Raman and X-ray Photoelectron Spectroscopy (XPS), X-ray Diffraction (XRD) and Atomic Force Microscopy (AFM). Photo-current and photo-electrochemical responses of the as-deposited and annealed films were investigated to evaluate their potential to be used in visible-light photocatalytic water splitting for hydrogen production.

2. Experimental details

Nitrogen-doped zinc oxide (ZnO_xN_y) thin films were grown at room temperature (no intentional substrate heating) on glass and copper substrates, using reactive HiPIMS. A pure Zn target (2 in. in diameter, 99.995% purity, from Kurt J. Lesker Company) was sputtered in a mixture of high purity Ar, N_2 and O_2 gases, keeping constant mass flow rates of 20, 10 and 1 sccm and a total gas pressure of 6.66 Pa. Prior to the deposition process, the substrates were cleaned in an acetone and ethanol mixture solution, under ultrasonic bath, for 15 min, followed by rinsing with de-ionized water and drying under nitrogen gas flow. Unipolar short voltage pulses (10 μs duration), with amplitude of −1 kV and very high instantaneous power density (~4 kW/cm^2 averaged over the racetrack area) were applied to the magnetron cathode, ranging the repetition frequency values over 350–800 Hz. The target-to-substrate distance was 6 cm and the deposition time was fixed to 60 min for all the samples. Details on the experimental set-up can be found in one of our previous works [6]. The obtained films were studied in as-deposited state and after annealing at 500 °C in nitrogen atmosphere.

The structural and surface topological properties of both as-deposited and annealed films were studied by XRD (Shimadzu LabX XRD-6000 diffractometer, Cu K_α radiation, $\lambda = 0.15406$ nm, Bragg-Brentano configuration) and AFM (NT-MDT SolvePro microscope). Micro-Raman spectra of the films were recorded at room temperature, in backscattering configuration, using a 632 nm laser. The scattered light was detected by a water-cooled charge coupled device detector (LabRAM HR-800, Jobin Yvon). The nitrogen atom concentration and chemical bonding states in the as-deposited films were investigated by XPS (PHI 5000 VersaProbe system from ULVACPHI, Inc.). Optical properties were analyzed in the wavelength range of 300–1100 nm, using an UV–Vis spectrophotometer (Evolution 300 from Thermo Scientific). The optical band-gap of the ZnO_xN_y thin films was estimated from the Tauc plots of the optical transmittance. The thickness of the deposited films was estimated using a Quartz Crystal Microbalance (Inficon Q-pod), placed in the virtual substrate position, at a distance of 60 mm from the target's surface. The photoelectric response of the films deposited on glass substrates was investigated by measuring the photo-current (PC) under blue light illumination ($\lambda = (405 \pm 10)$ nm, power density of 0.7 mW/cm^2) in ambient air. The PC of the ZnO_xN_y films was measured by electrically connecting into a current-voltage measuring circuit two silver interdigital electrodes deposited on the films' surface by thermionic arc, using a comb-shaped mask (gap length of 3 mm and gap width of 0.2 mm). The obtained device was connected into an electrical circuit in order to measure both dark- and photo-current for 0.5 V voltage applied to the electrodes. The photo-current was measured using a picoampermeter (Keithley, Model 2612A) under direct illumination with blue light from a laser diode. The photo-electrochemical response, light excitation efficiency and photo-sensitivity of ZnO_xN_y films deposited on copper substrates were tested in a conventional three electrode arrangement electrochemical cell with aqueous electrolyte solution (0.1 M NaOH) under standard solar illumination conditions (AM 1.5 G, 100 mW·cm^{-2}). The experimental procedures and equipment for the photo-electrochemical measurements have been described in [9]. The Incident-Photon-to-Current-Efficiency (IPCE) has been calculated with following eq. [9]:

$$IPCE(\lambda) = \frac{h \cdot c}{\lambda} \cdot \frac{J_{ph}(\lambda)}{e \cdot P(\lambda)} (\%) \quad (1)$$

where $J_{ph}(\lambda)$ is the photo-current density, $P(\lambda)$ is the incident power density, λ is the wavelength of the incident light, h is the Planck constant (6.62×10^{-34} J·s), c is the light velocity (3×10^8 m/s), and e is the elementary charge (1.6×10^{-19}C).

In one of our previous works, we have described the ability of reactive HiPIMS technique to tailor the chemical composition and optical band-gap of the nitrogen containing zinc oxide through the pulsing scheme design [6]. Thus, increasing the pulse repetition frequency for the reactive HiPIMS of pure Zn target in $Ar/N_2/O_2$ gas mixture from 350 to 800 Hz allowed the deposition of polycrystalline ZnO_xN_y films with nitrogen content ranging from 0 to 6.2 at.% and the corresponding optical band-gap values ranged over 3.34–1.67 eV. In this work, a series of samples (labeled as S1 to S8), containing zinc oxide with different nitrogen concentrations, was deposited by HiPIMS on glass and copper substrates, at room temperature.

In Table 1 are listed the sputtering conditions, thickness, optical band gap values, surface roughness, visual aspect color and atomic percentage of nitrogen in the ZnO_xN_y deposited films. Structural, morphological, compositional and optical properties of the films deposited on glass substrates have been investigated by XRD, Raman spectroscopy, AFM, XPS and UV–Vis techniques. The photocatalytic activity, light excitation efficiency and photo-sensitivity of the oxynitrides films deposited on copper substrates under similar conditions, were investigated by photo-current and photo-electrochemical measurements.

3. Results and discussion

3.1. Thin film characterization

3.1.1. Chemical bonding states and structure

The nitrogen atom concentration and chemical bonding states in the as-deposited films were investigated by XPS measurements. The chemical composition was determined from the ratio of each peak area to the total peak area for Zn 2p, N 1s and O 1s peaks. Experimental results show that the nitrogen content of the deposited films can be finely tuned by changing only the pulse frequency. Thus, nitrogen concentration in the deposited films gradually increases with the pulse frequency, reaching about 6.2 at.% for a repetition frequency of 800 Hz (see Table 1). At high repetition frequency values, the discharge was operated in the metallic target sputtering mode with high sputtering rates. In this case, the large amount of sputtered metal atom in the gas phase and the limited amount of oxygen in the working gas mixture resulted in a deficit of oxygen in the deposited films, creating bonding sites between the Zn and the less reactive nitrogen atoms. At low frequency values, the discharge operates in reactive mode, the target is fully oxidized, and there is less N incorporation in the film.

High-resolution XPS spectra of the O 1s, N 1s and Zn 2p peaks of the films deposited at repetition frequency of 800 Hz (S1) are shown in Fig. 1. The higher binding energy component located at 532.6 eV is usually attributed to the presence of a $Zn(OH)_2$ phase in the deposited films. This phase might be a result of water vapour absorption from the atmosphere. The peak centered at 531.1 eV can be attributed to O—Zn bonds between O^{2-} ions on the wurtzite structure of the hexagonal Zn^{2+} ion array [10]. The N 1s peaks located at 397.7 eV and 400.4 eV may be ascribed to the anionic N^- in the N—Zn and N—H bonds, respectively [11]. The XPS analysis revealed that N_O—Zn and O—Zn bonds coexist in the films, N_O being formed by substituting a single O atom with N in the ZnO lattice. The core lines of Zn $2p_{3/2}$ and $2p_{1/2}$ are located at 1022.8 eV and 1045.85 eV, respectively, and no metallic Zn peak

Table 1
Parameters for the high-power impulse magnetron sputtering discharge and characteristics of the thin films deposited at different pulsing frequencies. After thermal annealing, the band-gap values have been slightly increased (for example for S1 sample, E_g increases with 0.1 eV).

Sample	S8	S7	S6	S5	S4	S3	S2	S1
Peak current (A)	30	28	27	26	25	24	22	20
Frequency (Hz)	350	400	450	500	550	600	700	800
Average power (W)	45	51	57	62	66	70	74	80
Thickness (nm)	550	750	1100	1400	1700	1900	2200	2540
N (at. %)	0.0	0.8	2.2	3.4	3.9	4.9	5.4	6.2
Band gap (eV)	3.34	3.3	3	2.35	2.1	1.9	1.75	1.67
Roughness (nm)	3.3	3	2.7	3.1	4	6	6.5	6.3
Colour	Transparent	Light yellow	Yellow	Orange	Light brown	Brown	Dark brown	Dark brown

(usually located at 1021.5 eV) was observed, indicating that in the deposited films, Zn exists only in the oxidized state [12].

The nitrogen incorporation in the ZnO lattice and crystal quality of the ZnO_xN_y films were further studied by micro-Raman analysis. Fig. 2 shows Raman spectra of the ZnO_xN_y films grown on glass substrates. Characteristic Raman modes of nitrogen doped ZnO can be observed in the presented spectra, indicating a good crystallinity of the ZnO_xN_y films. The Raman peaks located at 581 cm^{-1} A_1 (1LO) correspond to longitudinal optical modes of nitrogen doped ZnO [13]. The broad Raman peaks A_1 (2LO) located around 1162 cm^{-1} are attributed to the second order of the A_1 (1LO) modes. The higher intensity of A_1 (LO) modes coincides with the prediction of group theory which supports the better crystal quality of nitrogen doped ZnO films. The additional Raman mode at 275 cm^{-1} corresponds to the local vibrational modes of nitrogen in ZnO, being related to the substitution of N into O sites [14,15]. Therefore, besides a good crystallinity, the Raman spectra show clear evidence of substitutional nitrogen in the doped ZnO lattice.

The crystalline structure of the as-deposited (see Supporting Material in ref. [6]) and thermally annealed films was studied by XRD. The obtained results show that the un-doped and weak doped ZnO films possess high crystallinity with preferentially c-axis orientation. The strong diffraction peak located around $2\theta = 34.4°$ corresponds to (002) plane of hexagonal wurtzite ZnO structure. Increasing the nitrogen concentration in the deposited films leads to a change of orientation, while the diffraction trace of the (002) plane is evidently weakened and additional diffraction peaks appear. With further increase of the nitrogen content, the XRD patterns show intermixing phases of Zn_3N_2 [16] and $Zn(N_3)_2$ [17] structures. In Fig. 3(a) and (b) are illustrated Raman spectra (Fig. 3(a)) and XRD pattern (Fig. 3(b)) of as-deposited and thermal annealed ZnO_xN_y films deposited at 800 Hz pulsing frequency (S1). Both results indicate a slight increase of the film's crystallinity after thermal annealing.

3.1.2. Surface morphology

Since the photocatalytic activity of semiconductor thin films is determined by the processes taking place at films surfaces, an AFM investigation of the surface morphology of the ZnO_xN_y thin films deposited on glass substrates is worthwhile. In order to analyze and compare the surface roughness of the deposited films with different nitrogen content, three random areas (3 μm × 3 μm) over the surface of each deposited film were scanned with the same AFM probe (nominal tip apex

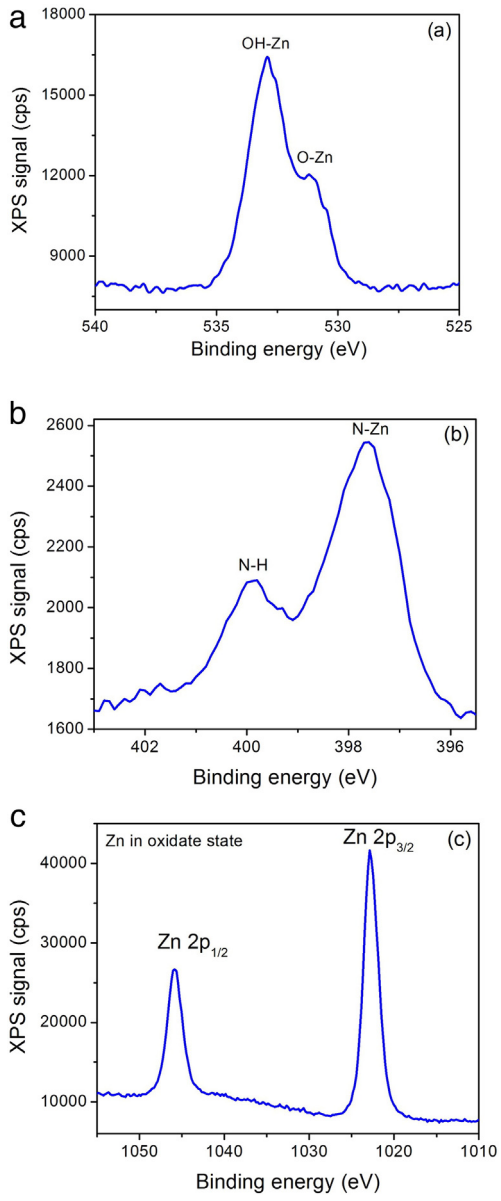

Fig. 1. High-resolution XPS spectra of: (a) O 1s, (b) N 1s, and (c) Zn 2p lines, for ZnO_xN_y films deposited on glass substrates at pulsing frequency values of 800 Hz (S1).

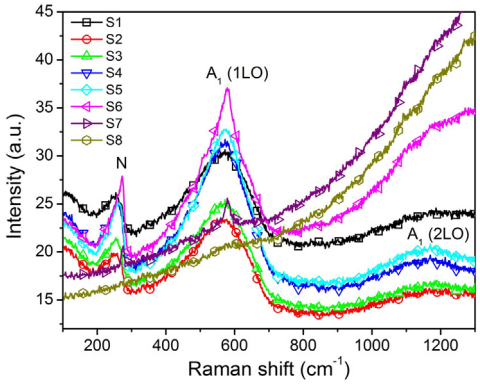

Fig. 2. Room temperature Raman spectra of as-deposited ZnO_xN_y samples excited with 630 nm.

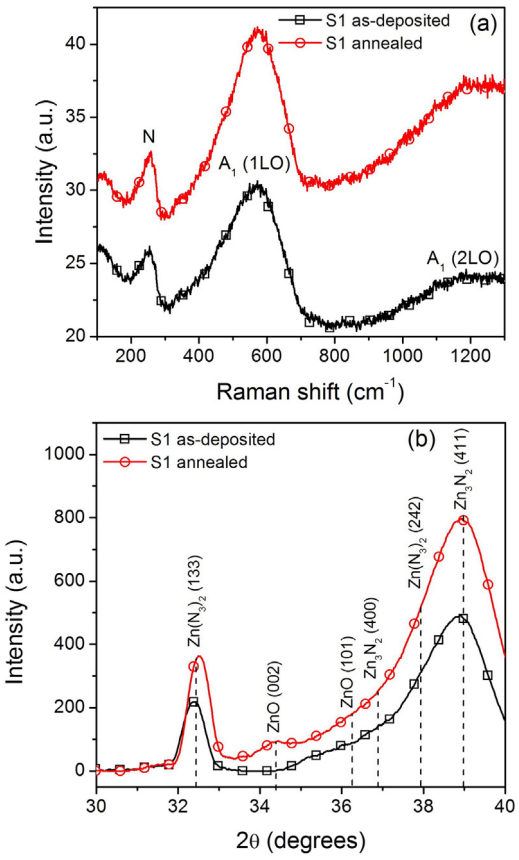

Fig. 3. Raman spectra (a) and XRD patterns (b) of as-deposited and thermal annealed ZnO_xN_y films deposited at 800 Hz pulsing frequency (S1).

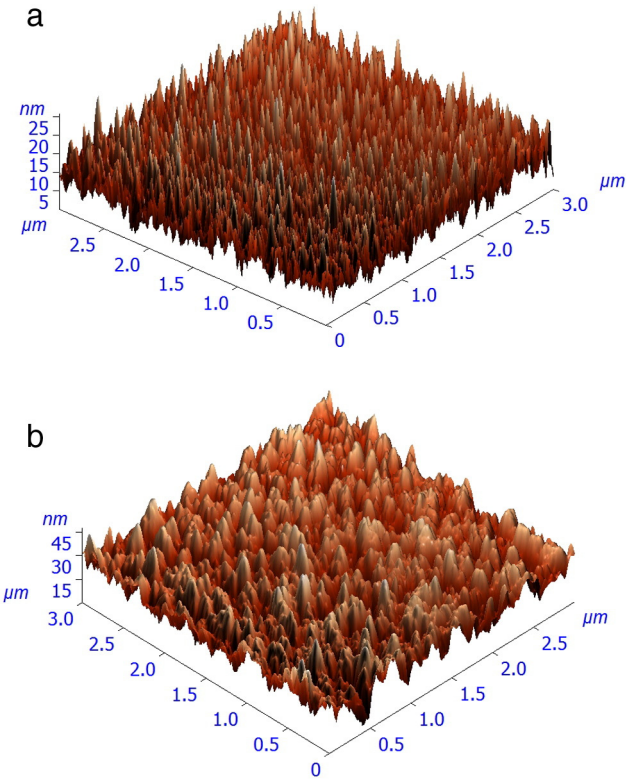

Fig. 4. 3D AFM images of as-deposited ZnO_xN_y thin films deposited on glass substrates at: (a) 350 Hz and (b) 800 Hz pulsing frequency.

curvature of 10 nm). The average grains size and root mean square (RMS) surface roughness values were calculated using image processing software. The AFM scan of the films surfaces indicated a prevailing grain-like surface morphology, with grain homogeneously distributed. The same results revealed that the RMS roughness and grain size of the ZnO_xN_y thin films increased with the nitrogen content, i.e. with the increasing of the pulsing repetition frequency. As resulted from the analysis of the AFM micrographs of the as-deposited films, increasing the pulsing frequency from 350 to 800 Hz, the RMS surface roughness value increased from 2.7 ± 0.5 to 6.5 ± 0.5 nm, while the mean lateral size of the grains increased from 25 to 80 nm. Fig. 4(a) and (b) present 3D images of surface topography of as-deposited ZnO_xN_y thin films deposited on glass substrates at pulsing frequency 350 Hz and 800 Hz, respectively. A slight increase in the grain size, as a result of the annealing treatment, was observed. This modification of surface morphology is an indicator of changes in internal mesostructure of the film as a result of the annealing process.

3.1.3. Optical properties

The optical properties of the films were interpreted from their transmittance spectra recorded using an UV–Vis spectrophotometer. Optical transmittance spectra recorded in the wavelength range from 300 to 1100 nm are shown in Fig. 5. It is noteworthy that, in these measurements, the bare substrate was placed in the reference path of the beam and, hence, the values from Fig. 5 correspond to the film transmittance alone. As the pulse repetition frequency increases, the content of nitrogen in the as-deposited films increases and the optical adsorption edge is shifted towards longer wavelengths. The band-gap energy of the ZnO_xN_y films was calculated from the linear fit of the linear part of the $(\alpha h\nu)^2$ vs. $h\nu$ plot (direct band-gap semiconductor). The obtained results indicate that the energy band-gap (E_g) gradually decreases from 3.34 eV (for the films with no content of N) to 1.67 eV (for the films with 6.2 at.% content of N). The lower E_g values can be related to the variation of N content in the films, as well as to the formation of Zn—N bonds which have lower ionicity compared to the Zn—O bonds [18].

From the results of XPS, Raman, XRD and UV–Vis measurements, it was found that the nitrogen concentration in ZnO_xN_y films increases up to 6.2 at.%. This variation of chemical composition causes changes in the micro-structural and optical properties of the films.

3.2. Photo-electrochemical characterization

The photo-electrochemical (PEC) properties and photocatalytic activity of as-deposited and annealed ZnO_xN_y films were evaluated by

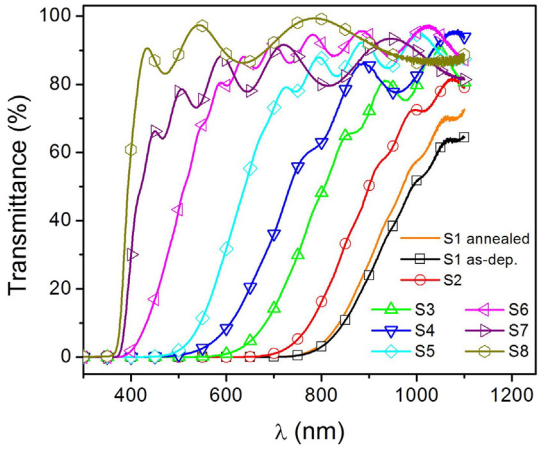

Fig. 5. Optical transmittance spectra recorded at room temperature for as-deposited ZnO_xN_y films sputtered on glass substrate at selected values of pulsing frequency (pulse width of 10 μs, O_2, N_2 and Ar flow rates of 1, 10 and 20 sccm, respectively).

using them as photoanodes for water splitting reaction. The as-deposited films showed a very weak PEC response towards water splitting. However, the PEC response has been significantly enhanced as a result of the annealing process of the films, performed for 60 min, in nitrogen atmosphere, at 500 °C. Compared with the films with lower or higher content of nitrogen, the ZnO_xN_y film (S5, 3.4 at.% nitrogen, E_g = 2.35 eV) showed the best photocatalytic activity after the post-deposition annealing treatment. Fig. 6 shows the comparison of PEC responses of as-deposited and annealed S5 film illuminated by time-chopped light (sunlight simulated by a xenon lamp, see ref. [9]). The spike decay towards the steady-state in the photo-current response during illumination period indicates a high rate of recombination processes in the films [19]. The very sharp photo-current spikes, present in the chopped-light curve when the light is turned on, denote a high density of undesirable surface states (crystalline defects and oxygen vacancies) acting as recombination sites for photo-generated carriers [20].

For the as-deposited films, a very small photocurrent, defined as the difference between dark and illumination currents, was observed. It was also noticed that the as-deposited films were not stable during PEC measurements, being etched by NaOH solution. Therefore, the measurement of the Incident-Photon-to-Current-Efficiency (IPCE) of as-deposited films was not possible. The low photocatalytic activity of as-deposited films has been attributed to the presence of defect states (e.g. oxygen vacancies) in their crystal structure. Consequently, in order to improve their crystalline order and photocatalytic activity, the samples were subjected to thermal treatments. After the thermal annealing process, the photo-current response was considerably improved, the PEC intensity increasing under illumination with simulated sunlight towards values as high as 100 μA/cm^2 at 0.5 V vs. Ag/AgCl determining the maximum IPCE up to 33% at λ = 370 nm (Fig. 7). The IPCE decreases almost linearly between 370 and 640 nm, showing a cut-off at 640 nm.

Using hydrothermal method, Yang et al. [5] synthesized nitrogen-doped zinc oxide nanowire arrays with better activity in UV light, but with much lower activity in the visible light. For the same potential value (0.5 V vs. Ag/AgCl) and a wavelength of 400 nm, they reported an IPCE value of 15% and a cutoff wavelength at 450 nm. Using sol-gel and HiPIMS depositions, Krysa et al. [21] obtained titanium oxide (TiO_2) and iron oxide (α-Fe_2O_3) hematite films with potential applications as photoanodes in electrochemical water splitting. They compared the best Fe_2O_3 and TiO_2 films and found that, at λ = 365 nm, the IPCE, measured at 1.6 V vs. Ag/AgCl, reached values of 17.3% and 8.2%, respectively, while, at 404 nm, the IPCE was 9.4% for Fe_2O_3 and negligible for TiO_2. Recently, Valerini et al. [22] deposited, by RF magnetron sputtering, tungsten oxide (WO_3) thin films for potential applications

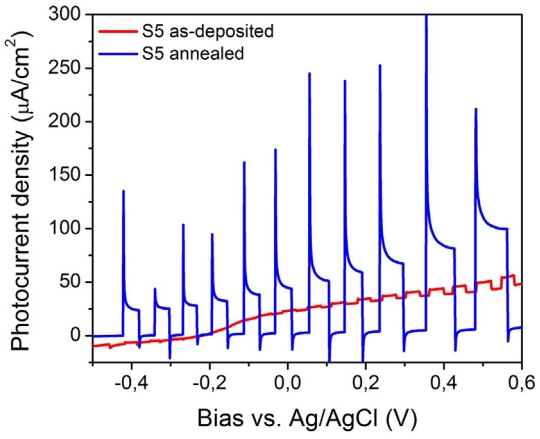

Fig. 6. Chopped light polarization curves of as-deposited and annealed ZnO_xN_y thin films with 3.4 at.% nitrogen concentration (incident light flux of 100 mW, electrolyte 0.1 M NaOH, scan rate of 50 mV·s^{-1}).

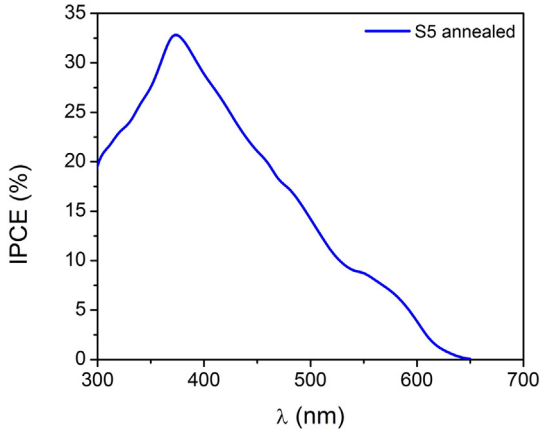

Fig. 7. Incident-Photon-to-Current-Efficiency (IPCE) measured at 0.5 V vs. Ag/AgCl for annealed ZnO_xN_y thin films with 3.4 at.% nitrogen concentration.

in water splitting. They found a maximum IPCE of 15% at 320 nm for 0.6 V vs. Ag/AgCl, and a cutoff wavelength at 410 nm.

The nitrogen content in zinc oxynitride thin film has an important role on the photocatalytic activity improvement for water molecule splitting under visible light irradiation, due to the effect on the optical band-gap energy, resulting in red-shifting of the absorption spectra. However, besides improving the absorption spectra in visible light, a high content of nitrogen may also impede the formation of crystalline phases in the deposited films with the unwanted effect of generation of recombination sites for the photo generated charge carriers. Our films structure investigations showed a decrease in the crystalline order of ZnO_xN_y films with increasing the nitrogen content. Thus, the Raman spectroscopy results showed that A_1 (1LO) mode, which indicates the presence of a high density of oxygen vacancies or zinc interstitials in the film, increases with the increase of the nitrogen content in the films. Lowering the crystalline order determines poor photocatalytic activity because of the occurrence of many recombination and trapping centers for the photogenerated holes and electrons. However, post-deposition annealing treatment improved the crystalline order in the films, probably by reducing the density of oxygen vacancies [23]. Therefore, the enhanced PEC response of the annealed films may be related to the reduction in defect density.

3.3. Photo-current characterization

In order to understand the effect of annealing treatment on the photocatalytic activity and the differences between the photocatalytic activities of the films with various nitrogen contents, we have performed measurements of photoelectric response of three selected samples (S4 with 3.9 at.% of N, S5 with 3.4 at.% of N and S6 with 2.2 at.% of N), illuminated with visible light (λ = 405 ± 10 nm). The dark photo-current, measured between the interdigital electrodes deposited on the films surface, showed a linear dependence on the applied voltage (not shown here), indicating a good Ohmic contact between the silver electrodes and the ZnO_xN_y films. The transient PC during blue (λ = 405 ± 10 nm) light illumination on-off cycles was measured in ambient atmosphere using a bias voltage of +0.5 V. The as-deposited films (Fig. 8) showed very weak photo-conducting behaviour (PC intensity ≈ 10 μA). However, the PC response enhanced very much as a result of the post-deposition annealing treatment of ZnO_xN_y thin films, performed in nitrogen environment, at 500 °C, for 60 min. The UV–Vis, Raman and XRD investigations revealed a slight increase of energy band gap (around 0.1 eV) and a slight improvement of crystalline order for the annealed thin films as compared to the as-deposited ones. This proved that the annealing treatment removed charge carrier recombination centers (defects in the micro crystalline structure of the as-deposited films), without essentially changing the film composition and mesoscopic structure. After thermal

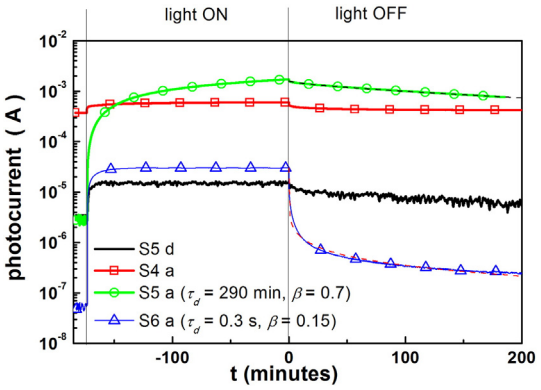

Fig. 8. Transient photo-current intensity of ZnO_xN_y films with different nitrogen content during an on–off cycle of the blue light (405 ± 10 nm) irradiation (as deposited film S5d and annealed films S4a, S5a and S6a). Time variations of the photo-currents during time-off period of light irradiation were fitted with stretched exponential decay described by Eq. (2) (fitting plots are shown only for the annealed films S5a and S6a).

annealing, the films exhibited a pronounced photo-conducting behaviour, the measured photo-currents being very high as compared to those of the as-deposited films. Fig. 8 shows the photo-current intensity during an on–off cycle of the blue light irradiation of as-deposited and annealed ZnO_xN_y films, with different nitrogen content.

Neglecting surface recombination and considering that the electron–hole recombination rate in the bulk was determined by electron diffusion [24], the decay of charge charier density (and photocurrent), during the off-time of the light irradiation cycle, may be described by a stretched exponential:

$$I = I_0 \cdot \exp\left[-(t/\tau_d)^{\beta}\right] \quad (2)$$

where $I(t)$ is the photo-current intensity at time t (measured from the moment of switching off the light irradiation), I_0 is the initial photo-current intensity, τ_d is the effective decay time of charge carriers and β ($0<\beta<1$), is the dispersion parameter. Fitting the experimental data, obtained for the as-deposited and annealed S5 film, with Eq. (2) determined values of 170 s and 290 s for τ_d and 0.36 and 0.7 for β, respectively. Therefore, the annealing treatment process resulted in an increase in the τ_d and β values, due to the improvement of crystalline order in the film. It is well known that the recombination time for photo-induced charge carriers in indirect band semiconductors as TiO_2, is very long [25], this being one of the causes of the very good photocatalytic activity of this material. However, the recombination time of charge carriers in a direct gap semiconductor as ZnO is much shorter, but it increases exponentially with the energy band bending at grain interfaces [26]. On the other hand, ZnN has been identified as an indirect band-gap semiconductor [27], so that an increase in the recombination time of charge carriers with the increase of nitrogen content in ZnO_xN_y thin films is expected. Trapping and separation of charge carriers in nanocrystalline semiconductor films is also expected to significantly increase the recombination time [28]. Long lifetime of photo-induced charge carriers is beneficial for the photocatalytic activity, because charge carriers are available for surface reactions for longer time. However, separation of charge carriers can prevent not only charge recombination, but also participation of either electrons or holes to the surface photocatalytic reactions [29].

The transient photo-conductivity measurements of the annealed ZnO_xN_y films during on–off cycle of the blue light irradiation show the best photo-response (highest photo-current intensity and longer life time of the electrical charge carriers) for the S5 sample, which also showed the best photocatalytic activity for water splitting under visible light irradiation. After the blue light irradiation was turned on, the photo-current intensity showed a fast increase, followed by a slow rise towards a stationary value. This stationary value was very different for the three selected ZnO_xN_y thin films, the larger value being observed for the annealed film with the best photocatalytic activity (S5). The stationary value of the photo-current depends on the dynamic balance between charge carrier production (photogeneration) and consumption (bulk and surface recombination and surface reactions with adsorbed oxygen and water molecules). At the same generation rate, the longer the life time of the photogenerated charge carriers is, the higher stationary value of the photogenerated current intensity is. Indeed, the expanded exponential decay of the photo-current during irradiation-off time for the S5 film also showed the highest life time values for the photogenerated charge carriers in this film. The S4 film showed the highest dark current (high conductivity), probably due to a large number of free electrons from Zn atoms in lower oxidation states. The S6 film, with lower content of nitrogen and larger band-gap energy, showed the lowest dark current intensity and also the lowest photo-current intensity. This behaviour may be explained by lower photogeneration rate of charge carriers (due to the increased band-gap energy) and the shortest life time ($\tau_d = 0.3$ s) of photogenerated carriers in this film. The increase of the nitrogen content in the film may be associated with a large density of defects in the polycrystalline structure of this film (indicated by the low β value of this film, $\beta = 0.15$), which acts as bulk and surface charge carrier recombination centers. The photo-response curve of this film shows, in an initial stage, a very rapid photo-current increase which corresponds to a rapid process of photo-generation of electron–hole pairs, followed by a second stage of a very slow growth process, which may be attributed to the surface photo-desorption of oxygen and water molecules. Similarly, when the light is turned off, the photo-current shows a rapid decay due to the electron–hole recombination, followed by a slow decay, which corresponds to the oxygen and water adsorption on the film's surface [30]. The high photo-current intensity obtained under light illumination, as well as the slow decay of the photo-current during dark conditions, are features of a good photocatalytic film. The difference in the lifetime of the photo-induced charge carriers may be explained by the different crystalline structure and density of charge carrier recombination sites in the films [30].

4. Conclusion

We have investigated the ability of reactive High Power Impulse Magnetron Sputtering (HiPIMS) deposition technique to synthesize ZnO_xN_y thin films with good photocatalytic activity for water splitting under visible light irradiation. HiPIMS operated with various values of pulsing frequency allowed the deposition of zinc oxinitride (ZnO_xN_y) thin films with variable content of nitrogen and corresponding optical band-gap energy values ranged between 3.34 eV (low content of nitrogen in the deposited films) and 1.67 eV (high content of nitrogen in the deposited films). However, despite the good absorbance in the visible light, the as-deposited films showed a very poor photocatalytic activity and chemical instability in NaOH aqueous electrolyte. The photocatalytic activity and chemical stability were considerable improved by a post-deposition thermal annealing treatment, performed in nitrogen atmosphere. According to the photo-current and photo-electrochemical characterization, the best photo-current response and photocatalytic activity has been obtained for the annealed ZnO_xN_y thin films with 3.4 at.% nitrogen concentration and an optical band-gap of 2.35 eV. The IPCE measurements of these films (33% at $\lambda = 370$ nm and 0.5 V biasing potential vs. Ag/AgCl) confirmed their high visible light activity and recommend them as excellent candidates for solar-assisted water splitting applications. The ZnO_xN_y films with higher content of nitrogen showed a poorer photocatalytic activity and stability due to a lower crystalline order in their structure, even after the annealing treatment process. On the other hand, the ZnO_xN_y films with smaller content of nitrogen showed poorer photocatalytic activity in visible light due to their larger band-gap energy and poor photogeneration of charge carriers

Please cite this article as: V. Tiron, et al., Surf. Coat. Technol. (2016), http://dx.doi.org/10.1016/j.surfcoat.2016.11.087

under visible light irradiation. Fabrication of stable and efficient visible-light photocatalytic ZnO_xN_y thin films requires further efforts for optimization of the reactive HiPIMS synthesis and post-deposition annealing processes.

Acknowledgment

This work has been supported by the Romanian National Plan for Research, Development and Innovation, grant PN-II-PT-PCCA-2011-3.2-1340, no. 174/2012 and JOINT RESEARCH PROJECTS - PN-II-ID-JRP-2012- RO-FR-0161.

References

[1] K. Maeda, Photocatalytic water splitting using semiconductor particles: history and recent developments, J Photochem Photobiol C: Photochem Rev 12 (2011) 237.
[2] K. Kamata, K. Maeda, D. Lu, Y. Kako, K. Domen, Synthesis and photocatalytic activity of gallium-zinc-indium mixed oxynitride for hydrogen and oxygen evolution under visible light, Chem. Phys. Lett. 470 (2009) 90.
[3] X. Ye, L. Qi, Two-dimensionally patterned nanostructures based on monolayer colloidal crystals: controllable fabrication, assembly, and applications, Nano Today 6 (2011) 608.
[4] S. Sakthivel, M.V. Shankar, M. Palanichamy, B. Arabindoo, D.W. Bahnemann, V. Murugesan, Enhancement of photocatalytic activity by metal deposition: characterization and photonic efficiency of Pt, Au and Pd deposited on TiO_2 catalyst, Water Res. 38 (2004) 3001.
[5] X. Yang, A. Wolcott, G. Wang, A. Sobo, R.C. Fitzmorris, F. Qian, J.Z. Zhang, Y. Li, Nitrogen-doped ZnO nanowire arrays for photoelectrochemical water splitting, Nano Lett. 9 (2009) 233.
[6] V. Tiron, L. Sirghi, Tuning the band gap and nitrogen content of ZnO_xN_y thin films, Surf. Coat. Technol. 282 (2015) 103.
[7] V. Tiron, L. Sirghi, G. Popa, Control of aluminum doping of ZnO:Al thin films obtained by high-power impulse magnetron sputtering, Thin Solid Films 520 (2012) 4305.
[8] V. Tiron, I.-L. Velicu, A. Demeter, M. Dobromir, F. Samoila, C. Ursu, L. Sirghi, Reactive multi-pulse HiPIMS deposition of oxygen-deficient TiO_x thin films, Thin Solid Films 603 (2016) 255.
[9] M. Rioult, H. Magnan, D. Stanescu, A. Barbier, Single crystalline hematite films for solar water splitting: Ti-doping and thickness effects, J. Phys. Chem. C 118 (2014) 3007.
[10] B. Yang, P. Feng, A. Kumar, R.S. Katiyar, M. Achermann, Structural and optical properties of N-doped ZnO nanorod arrays, J. Phys. D. Appl. Phys. 42 (2009) 195402.
[11] J.G. Ma, Y.C. Liu, R. Mu, J.Y. Zhang, Y.M. Lu, D.Z. Shen, X.W. Fan, Method of control of nitrogen content in ZnO films: structural and photoluminescence properties, J. Vac. Sci. Technol. B 22 (2004) 94.
[12] M.N. Islam, T.B. Gosh, K.L. Chopra, H.N. Acharya, Thin Solid Films 280 (1996) 20.
[13] Y.G. Wang, S.P. Lau, X.H. Zhang, H.W. Lee, H.H. Hng, B.K. Tay, J. Cryst. Growth 252 (2003) 26.
[14] A. Kaschner, U. Haboeck, M. Strassburg, M. Strassburg, G. Kaczmarczyk, A. Hoffmann, C. Thomsen, A. Zeuner, H.R. Alves, D.M. Hofmann, B.K. Meyer, Nitrogen-related local vibrational modes in ZnO:N, Appl. Phys. Lett. 80 (2002) 1909.
[15] W.W. Liu, B. Yao, Z.Z. Zhang, Y.F. Li, B.H. Li, C.X. Shan, J.Y. Zhang, D.Z. Shen, X.W. Fan, Doping efficiency, optical and electrical properties of nitrogen-doped ZnO films, J. Appl. Phys. 109 (2011) 093518.
[16] M. Futsuhara, K. Yoshioka, O. Takai, Thin Solid Films 322 (1998) 274.
[17] H. Winkler, H. Krischner, Preparation & X-ray data of α-zinc Azide [α-$Zn(N_3)_2$], Indian J. Chem. 13 (1975) 661.
[18] M. Futsuhara, K. Yoshioka, O. Takai, Optical properties of zinc oxynitride thin films, Thin Solid Films 317 (1998) 322.
[19] L.M. Peter, Energetics and kinetics of light-driven oxygen evolution at semiconductor electrodes: the example of hematite, J. Solid State Electrochem. 17 (2013) 315.
[20] Z. Hubicka, S. Kment, J. Olejnicek, M. Cada, T. Kubart, M. Brunclikova, P. Ksirova, P. Adamek, Z. Remes, Deposition of hematite Fe_2O_3 thin film by DC pulsed magnetron and DC pulsed hollow cathode sputtering system, Thin Solid Films 549 (2013) 184.
[21] J. Krysa, M. Zlamal, S. Kment, M. Brunclikova, Z. Hubicka, TiO_2 and Fe_2O_3 films for Photoelectrochemical water splitting, Molecules 20 (2015) 1046–1058.
[22] D. Valerini, S. Hermandez, F. Di Benedetto, N. Russo, G. Saracco, A. Rizzo, Mater. Sci. Semicond. Process. 42 (2016) 150–154.
[23] S. Dhara, P.K. Giri, Stable p-type conductivity and enhanced photoconductivity from nitrogen-doped annealed ZnO thin film, Thin Solid Films 520 (2012) 5000.
[24] K. Sakaguchi, K. Shimakawa, Y. Hatanaka, Transport and recombination of photocarriers under potential fluctuation in TiOx films prepared by rf magnetron sputtering method, Phys. Status Solidi C 8 (2011) 2796–2799.
[25] L. Sirghi, Plasma synthesis of photocatalytic TiOx thin films, Plasma Sources Sci. Technol. 25 (2016) 033003.
[26] R. Yukawa, S. Yamamoto, K. Ozawa, M. Emori, M. Ogawa, S. Yamamoto, K. Fujikawa, R. Hobara, S. Kitagawa, H. Daimon, H. Sakama, I. Matsuda, Electron-hole recombination on ZnO(0001) single-crystal surface studied by timeresolved soft X-ray photoelectron spectroscopy, Appl. Phys. Lett. 105 (2014) 151602.
[27] F. Zong, H. Ma, W. Du, J. Ma, X. Zhang, H. Xiao, F. Ji, C. Xue, Optical band gap of zinc nitride films prepared on quartz substrates from a zinc nitride target by reactive rf magnetron sputtering, Appl. Surf. Sci. 252 (2006) 7983–7986.
[28] K. Sakaguchi, K. Shimakawa, Y. Hatanaka, Dynamic responses of photoconduction in TiO_x films prepared by radio frequency magnetron sputtering, Jpn. J. Appl. Phys. 49 (2010) 091103.
[29] L. Sirghi, Y. Hatanaka, Hydrophilicity of amorphous TiO_2 ultra-thin film, Surf. Sci. 530 (2003) L323.
[30] L. Sirghi, Y. Hatanaka, T. Aoki, Photocatalytic chemisorption of water on titanium dioxide thin films obtained by radio frequency magnetron deposition, Appl. Surf. Sci. 244 (2005) 408.

Please cite this article as: V. Tiron, et al., Surf. Coat. Technol. (2016), http://dx.doi.org/10.1016/j.surfcoat.2016.11.087